International Journal of analytical and Numerical Methods in Mechanical Design
Winter & Spring 2023 Vol 2 , Issue 1, 15-27

Permeability Variation and Fracture/Crack Effects in Concrete/Rocks based on Multi-laminate Model

Farzad Peyman [a,] ✉

[a] Faculty of Civil Engineering, Islamic Azad University, Qazvin Branch, Qazvin, Iran
Received 20 February 2023; Revised 10 March 2023; Accepted 28 April 2023
✉ f.peyman@srbiau.ac.ir

Abstract

The permeability matrix of rock is a physical/mechanical characteristic that closely relates to the microstructure of this heterogeneous geomaterial, and the orientation of micro-cracks led to some naturally existing micro-cracks. Upon the effects of loading/unloading and high-temperature development, micro-cracks appear in critical zones of rock media that can effectively change the conductivity against gas or other fluids. Finally, macro cracks are generated and increase the porosity of the rock matrix on the distribution and geometrical arrangement. Consequently, the permeability becomes higher and depends on the stress/strain level of the rock body during loading/unloading and the passing fluidity interaction process. The influence of stress level and high temperature on rock's gas and water permeability has been studied in the literature. Fractured rock formations show vastly different properties, such as adsorption, etc., concerning permeability and storage capacity, thus giving rise to mass exchange processes between fractures and the surrounding matrix. This interaction between fracture and matrix impacts the flow and transport processes in the fractured subsurface, which can be observed on each scale considered for investigation purposes. The influence of fracture-matrix interaction has to be scrutinized upon the planned tests conforming to the natural condition when dealing with safety investigations or remediation possibilities. This paper shows some of the effects of fracture-matrix interaction and its geometry on groundwater flow in a saturated fractured rock/concrete media and the parameters describing those processes concerning different scales. A damage model concept contains fracture network generation, mesh generation, and appropriate discretization techniques based on presumed sampling between planes and polygons. The influence of a polygon matrix of finite porosity on the effective hydraulic conductivity tensor of a fractured system is illustrated by an example. In this research, we focus on determining the gas and water permeability of rock commonly used in transportation works, including loose/low strength and high strength/dense rock/concrete in interaction with pre-peak stress and damage level in post-peak behavior of rocks.

Keywords: Fracture-matrix-interaction, crack opening, damage model, multi-laminate framework, conductivity coefficient

1. Introduction

Crack opening in brittle porous media such as concrete and rocks governs many fluid transfer properties that play a pivotal role in durability analyses. Instead of combining continuum and discrete models in computational analyses, it would be attractive to derive an estimate of crack opening from the continuum approach without considering the explicit description of a discontinuous displacement field in the constitutive and computational model.

The crack opening is a crucial parameter for many concrete structures to estimate durability. Cracks are preferential paths along which fluids or corrosive chemical species may penetrate inside concrete structural elements. For structures such as confinement vessels, for instance, tightness to gas or liquids is a major serviceability criterion governed by Darcy's law in which material permeability is involved. The material permeability is strongly related to the amount and orientation of cracking in concrete: permeability grows significantly as distributed micro-cracking develops (see, e.g., Choinska et al. 2007), and it jumps several orders of magnitude upon macro-cracking (Sugiyama et al. 1996, Hearn, N. 1999 and Hearn, N., & Lok, G. 1998). According to Poiseuille's law, the permeability of a cracked structure (with a single crack) is proportional to the square of the crack opening. Hence, predicting the durability of structural components requires models that damage has been localized.

Enhanced continuum and integral damage models are capable of representing diffuse damage, crack initiation, and possibly crack propagation (Pijaudier-Cabot, G., & Jason, L. 2002 and Pijaudier-Cabot, G. and Bazant, Z. 1987 and Peerlings et al. 1996 , 2001). They regard cracking as an ultimate consequence of a gradual loss of material integrity. These models, however, do not predict crack opening and orientation as they rely on a continuum approach to fracture.

Some fictitious crack models are based on explicitly describing the discontinuity within the material (e.g., the cohesive crack model of Hillerborg et al. 1976). They relate the crack opening to the stress/strain level and are based on linear elastic (or plastic) fracture mechanics. Cohesive crack models need proper algorithms for crack propagation, and more importantly, they cannot describe crack initiation.

The heterogeneous properties of such geological systems strongly influence flow and transport processes in fractured porous concrete and rock. Under saturated conditions, fractures are usually characterized by a

comparatively high permeability and a low storability and, therefore, represent preferential pathways to a rapid migration of fluids. In contrast, the surrounding concrete/rock matrix shows a relatively low permeability and a high storage capacity. Fluids entering the matrix by diffusive processes may cause long-term chemical aggression to the system by advancing slowly in the low–mobility matrix or by reentering the fractures. This interaction between fracture and matrix plays a significant role in fluid transport processes. Field tests like tracer or pumping tests and laboratory investigations provide some data necessary to examine flow and transport conditions. However, while the data received from field tests are usually not detailed enough to assess the behavior of a fractured aquifer, the data achieved from laboratory experiments are not likely to represent larger scales regarding the system's heterogeneity. Within the research project "Aquifer Analogy," laboratory and field experiments with fractured sandstone and numerical simulations with different model concepts are performed to formulate up-scaling possibilities that allow the information gained from small-scale investigations to be included in regional-scale models.

The strong discontinuity approach initiated by Simo et al. (1993) and widely used over the last decade (e.g., Oliver et. 2002, Larsson et al. 1999) offers the possibility of merging in the same formulation a continuous damage model for the bulk response and a cohesive model for the discontinuous part of the kinematics. It is certainly a combination of continuum–discrete modeling that is sound from a theoretical point of view and appealing from the point of view of the physics of fracture. The issue in combining the continuum-based model for crack initiation and then a discrete crack model for propagation is the threshold upon which one switches from one analysis to the other. Usually, it is considered that discontinuity appears when damage, stresses, or strain energy reaches a certain threshold fixed beforehand, which remains arbitrary (Comi et al. 2007, Simone et al. 2003). As we will see further, one of the outcomes of the present model is to provide an indicator based on which the appearance of a discontinuity during a damage process can be defined with a given accuracy.

The work presented in this research describes the influence of fracture–matrix– interaction on flow through damaged concrete and transport conditions in the fractured subsurface and the resulting effective parameters. The concept of scales and effective parameters will be explained, and the modeling setup used for numerical investigations with a discrete model concept will be outlined. For example, the seepage transport in the cracked rib base of the Sefid-rood concrete dam has been investigated and presented. The piezometer readings after earthquake cracks have been compared with the proposed model results to show the model's capability.

2. General Permeabiliy Distributuin at a Location

The permeability coefficient as a second-order physical tensor value represents the capability of a porous medium against the flow, keeping potential pressure at a certain location relative to the other surrounding locations. Any anisotropy and non-homogeneity in porosity and void geometry change through a porous medium can change the permeability tensor. This tensor, similar to the stress/strain tensor, represents an ellipsoidal variation around a certain location upon the change of orientation, as shown in Figure 1.

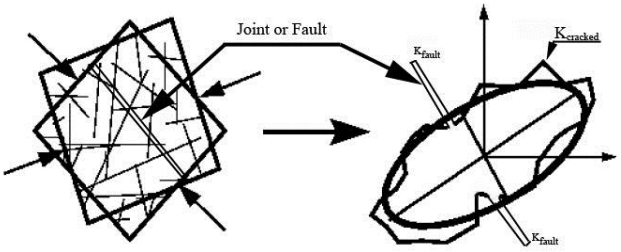

Fig.1. Initial elliptical anisotropy of permeability coefficient and fracture/cracks effects

Generally, the fracture–matrix – interactions and corresponding geometries influence the flow and transport processes and the effect on initial ellipsoidal permeability variation to an irregular/broken at a certain location through porous media. In real cases, the complexity of conductivity of a fractured concrete system, i.e., the disparity of the hydraulic properties of cracks/fractures and matrix combined with the irregular geometry of a fractured concrete, led to a more complex flow behavior.

3. Fracture–Matrix–Interaction

The influence of fracture–interaction and crack geometry on the effective permeability parameters used for computational purposes must reflect the flow direction tendency at a certain location conforming with the flow nature motion. It will be set out in the sequel with two aspects: the effective hydraulic conductivity tensor and the effective hydrodynamic dispersion affected mainly by inherent and induced fracture/cracking. The effective hydraulic conductivity tensor describes the permeability of a porous medium, respectively, of a fractured formation/crack progression, which has usually been subjected to an averaging process over a change in physical condition concerning fluid properties and gravitation. To determine the hydraulic conductivity tensor of a fracture-oriented network, the system is rotated concerning the pressure gradient, and for each rotation angle (Figure 1), the *K*-value is computed using the corresponding in- and outflow (Long, J. C. 1983). The more accurately the computed K-values fit into an ideal balancing ellipsoid, the better a porous medium with the corresponding conductivity tensor represents the fracture-oriented network. An effective hydraulic conductivity tensor can be determined by the same procedure for fracture–matrix–networks. However, considering a porous matrix in a fracture-oriented network affects the resulting hydraulic conductivity values in several ways. First, the porous matrix allows water to flow in the fractures/cracks and throughout the domain of interest.

Consequently, while rotating the domain concerning the pressure gradient, the resulting *K*-values fit more to a balancing ellipsoid than the *K* values of the corresponding pure fracture/cracked network would do. Second, the fracture-oriented network's connectivity plays a less important role when a matrix is involved. In contrast to

pure fracture-oriented networks in which a connective fracture/crack pathway from one edge of the domain to the other is a prerequisite for finding an effective conductivity value, fracture–matrix–systems can balance the missing fracture/crack connection by establishing flow pathways in the matrix. Third, any anisotropy of the matrix may influence the effective conductivity tensor of the fracture–matrix–system. The described effects depend primarily on the permeability difference between fracture quantity and its orientation and matrix and on the fracture density of the considered networks.

The quantity of effective dispersion has been introduced to describe the spreading of a fluid due to velocity fluctuations that arise from the heterogeneities of the underlying medium. Regarding the geometry of the single fracture, dispersive processes occur due to channeling effects in the rough fracture plane itself. If the single fracture is embedded in a matrix of finite porosity, the mass exchange between fracture and matrix must be considered. Depending on the porosity and the permeability of the matrix, and the pressure gradient between fracture and matrix, a considerable quantity of fluid will enter the matrix, leading to a strong tailing effect in the resulting breakthrough curve and a fast reduction of the concentration peak.

A similar behavior can be observed on the fracture orientation network scale. Water migrating through a fracture network will use different possible pathways of connected fractures, leading to a macroscopic dispersion effect. Suppose the mass exchange between the fracture network and a surrounding porous matrix is considered additionally. In that case, the resulting breakthrough curve will show a pronounced tailing while the corresponding concentration peak diminishes rapidly. The contrast between fracture and matrix properties may lead to completely different time scales for the solute migration rate in both system components. A description of the behavior of the breakthrough curves that presents results from fluid transport processes in fracture–matrix–systems by the employment of a multi-layer model presented by (Wollrath, J. 1990). Also, the analysis of the fluid flow behavior by evaluating spatial moments is presented by (Dagan, G. 2012).

4. Multi-Laminate Framework

Grains and paste in porous media such as concrete and sandstone materials consisting of contacts and surrounding voids are cemented particulate media that are mostly considered a continuum for ease. The accurate behavior of such particulate materials is to be investigated through micro-mechanics. However, the micro-mechanical behavior of cemented granular materials is inherently discontinuous and heterogeneous. The macroscopic as an overall or averaged behavior of cemented granular materials is determined by how discrete grains are arranged through a medium and by what kinds of interactions are operating among them. To investigate the micro-mechanical behavior of cementation and granular materials, the spatial distribution of contact points and orientation of grains must be identified. From an engineering point of view, the main goal is to formulate the macro-behavior of cemented granular materials in terms of micro-quantities. However, two well-known theories consistently explain the relation between micro-fields and macro-fields as macro-micro relations, as the average field theory and the homogenization theory.

The multi-laminate framework, by defining the small continuum structural units as an assemblage of particles and voids that fill infinite spaces between the sampling planes, has appropriately justified the contribution of interconnection forces in overall macro-mechanics. Upon these assumptions, plastic deformations are to occur due to sliding and separation/closing of the boundaries, and elastic deformations are the overall responses of structural unit bodies. Therefore, the overall deformation of any small part of the medium comprises total elastic response and an appropriate summation of sliding, separation/closing phenomenon under the current effective normal and shear stress/strain on sampling planes. These assumptions adopt overall sliding, separation/closing of inter-granular points of presumed grains included in one structural unit, which are summed up and contributed as the result of sliding, separation/closing surrounding boundary planes. This implies yielding/failure or even ill-conditioning and bifurcation response possible over any randomly oriented sampling planes. Consequently, plasticity control, such as yielding, should be checked at each plane, and those of the sliding planes will contribute to plastic deformation. Therefore, the granular material mass has an infinite number of yield functions, usually one for each of the planes in the physical space.

Figure 2 shows the arrangement of artificial polyhedrons simulated by real soil grains. The created polyhedrons are roughly by 13 sliding planes, passing through each point in the medium. The location of tip heads of normal to the planes defining corresponding direction cosines is shown on the surface of the unit radius sphere. In the ideal case, the normal integration is considered as summing up the individual micro effects corresponding to an infinite number of microsampling planes. The orientation of the sampling planes and direction cosines of two perpendiculars on plane coordinate axes and weighted coefficients for employed numerical integration rule and calculation of stress tensor of each plane are shown in Figure 3 and Table 1 (Peyman, F. 2022).

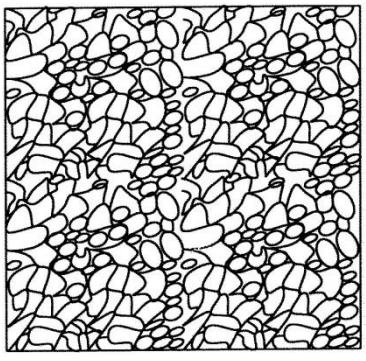

(a)

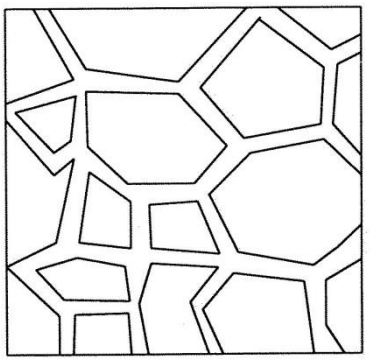

(b)

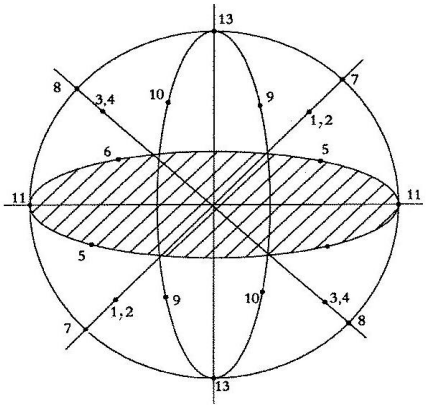

(c)

Fig.2. Concrete grains, artificial polyhedrons, and sampling points a) Real grains b) Polyhedrons c) Numerical integration points

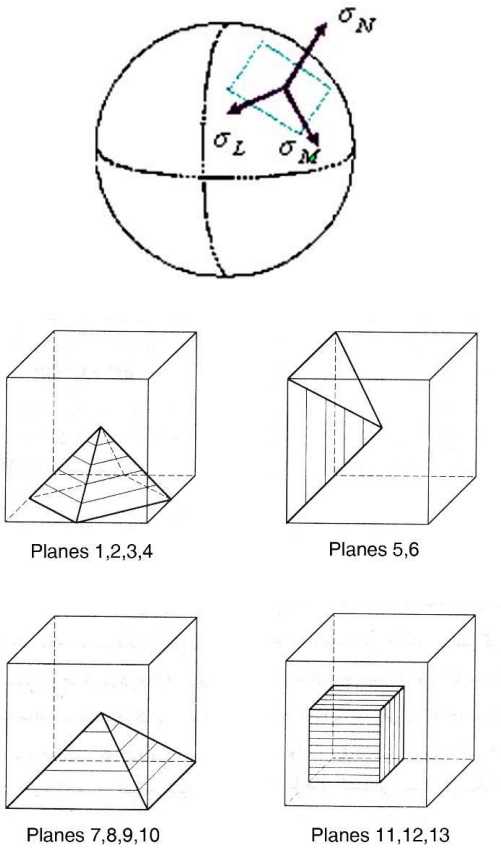

Fig.3. Definition and Projection of stress tensor on the unit sphere's surface

Table 1: Cosines of the normal axis and the weight coefficients for numerical integration

Plane No	Normal Axis			w_i
	l_i	m_i	n_i	
1	$\frac{1}{\sqrt{3}}$	$\frac{1}{\sqrt{3}}$	$\frac{1}{\sqrt{3}}$	$\frac{27}{840}$
2	$\frac{1}{\sqrt{3}}$	$-\frac{1}{\sqrt{3}}$	$\frac{1}{\sqrt{3}}$	$\frac{27}{840}$
3	$-\frac{1}{\sqrt{3}}$	$\frac{1}{\sqrt{3}}$	$\frac{1}{\sqrt{3}}$	$\frac{27}{840}$
4	$-\frac{1}{\sqrt{3}}$	$-\frac{1}{\sqrt{3}}$	$\frac{1}{\sqrt{3}}$	$\frac{27}{840}$
5	$\frac{1}{\sqrt{2}}$	$\frac{1}{\sqrt{2}}$	0	$\frac{32}{840}$
6	$-\frac{1}{\sqrt{2}}$	$\frac{1}{\sqrt{2}}$	0	$\frac{32}{840}$
7	$\frac{1}{\sqrt{2}}$	0	$\frac{1}{\sqrt{2}}$	$\frac{32}{840}$
8	$-\frac{1}{\sqrt{2}}$	0	$\frac{1}{\sqrt{2}}$	$\frac{32}{840}$
9	0	$-\frac{1}{\sqrt{2}}$	$\frac{1}{\sqrt{2}}$	$\frac{32}{840}$
10	0	$\frac{1}{\sqrt{2}}$	$\frac{1}{\sqrt{2}}$	$\frac{32}{840}$
11	1	0	0	$\frac{40}{840}$
12	0	1	0	$\frac{40}{840}$
13	0	0	1	$\frac{40}{840}$

When the on-plane stress condition exceeds the crack limits, sliding or widening/closing occurs as an active plane with progressing on-plane strain and cracking up to failure. Therefore, one of the important features of a multi-laminate framework is that it enables the identification of the activity, cracking, and failure planes as a matter of routine. The application of any stress path is accompanied by the actions of some of the 13 defined planes at any point in the medium. Plastic strain values on all the active planes are not necessarily the same. Some of these planes initiate plastic deformations earlier than others. These priorities and certain active planes can change due to any change of direction of the stress path; several active planes may stop the activity, some inactive ones become active, and some planes may take over others concerning the value of normal and shear strain. Thus, the framework can predict the cracked and final failure mechanism.

5. Tensor Quantities as Ellipsoidal Variable

A quantitative description of the initial micro-fabric would enhance the characterization and forecasting of anisotropic porous material behavior under different loading. These tensor quantities are naturally altered due to continuous loading changes. Hence, it is also necessary to develop techniques to quantify the changes in fabric. While the material is distorted, the fabric of the material changes, and so there is the strain or displacement field in the material. Consequently, the strain and induced fabric of a material and related corresponding tensor quantitative

such as permeability or flow conductivity are inherently related.

A popular approach for formulating tensor quantitative criteria for the anisotropy of porous materials is the generalization of isotropic ones. Such a criterion is usually geometrically interpreted as a limiting envelope in a strain/stress space, meaning that a failure condition occurs when a given strain/stress vector touches the failure envelope. Since the condition for failure is intrinsic to the material, the failure criterion can be defined differently for any probable sliding plane through the material. Accordingly, the strain/stress ratio cannot exceed the corresponding limit value on the planes of weakness or any other plane that does not tend to slide.

On a loading orientation inclined by three angles (direction cosines) concerning fracture orientation network or the bedding plane of natural porous media, a certain sliding mechanism composed of active sliding planes provides a value of strain/stress ratio, which corresponds to the most active plane and has a limitation of c and $\tan(\varphi)$ that is governing porous medium strength against sliding. Similarly, these criteria can be adopted for flow resistance of porous media that is permeability. Therefore, the Permeability matrix or flow conductivity at a single point initially has an ellipsoidal variation that any fracture/crack/fault can break locally to a higher level. Therefore, on any orientation within the porous media, the permeability state depends on the geometry and orientation of fracture/crack/joint. Flow speed distribution at a certain location is configured based on fracture/crack/joint orientations. To describe the permeability at any orientation, it is necessary to find a way of summarizing the configuration of different permeability corresponding to all the probable directions passing through any single point of the medium.

A spherical permeability envelope may provide uniform flow velocity on any orientation for ideal isotropic porous media with no preferential orientation. However, to consider fracture/crack/joint effects or even due to bedding plane, an irregular/broken ellipsoidal envelope of permeability may be the most suitable presentation of permeability variation in different directions. The longest diameter of this ellipsoid is always oriented along the major principal permeability direction, and the other medium and minor directions are normal to each other principal axes. Configuring the 13 predefined planes in permeability ellipsoid provides a certain elliptical section on each plane that presents the permeability variation concerning fracture/crack/joint orientations. In other words, the tips of the arrowhead of permeability value of different orientations collectively define a built-up geometrical surface called the permeability ellipsoid. The size of the permeability ellipsoid of each plane is different and presents maximum and minimum permeability for flow conductivity along the longest and shortest ellipse, respectively. The other flow conductivity orientations face permeability limitations depending on the direction of fracture/crack/joint on the plane concerning ellipsoid orientation.

Adopting the multi-laminate network mechanism of permeability, configured in Figure 3 concerning the orientation of the existing major principal permeability axis, these planes are configured symmetrically around a major principal axis. Any change in principal permeability axis direction creates a new set of permeability ellipses with different flow conductivity along fracture/crack/joint or sliding directions on different planes.

This study carried out for micro-fabric behavior of loose, medium, and dense granular materials led to the establishment of a statistical criterion of natural anisotropy based on hypotheses that experience accepted as probable. The fabric anisotropy law is represented as a spatial closed ellipsoid permeability function in x, y, and z coordinates as follows:

$$\frac{x^2}{B}+\frac{y^2}{B}+\frac{z^2}{A}=0 \qquad (1)$$

A, B, and C are three mutually perpendicular diameters of the ellipsoid. A construction of a typical ellipsoid is shown in Figure 4.

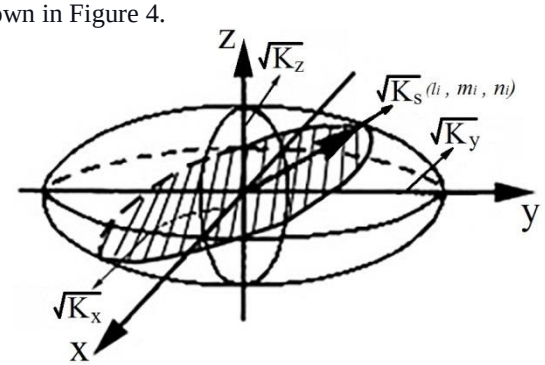

Fig.4. Initial permeability ellipsoid and planes

Furthermore, to overcome the fracture/crack/joint anisotropy concerns the effects of loading orientation, a possible having all different probable micro-crack widening/closing/sliding mechanisms must be provided in the used model. In this way, applying any arbitrary loading or strain/stress path leads to a certain crack/sliding mechanism that obeys the minimum energy level in natural law. These possibilities are provided in a nonlinear constitutive multi-laminate model (Sadrnejad, S. A. 1992, June, Peyman, F. 2022, Sadrnejad, S. A. (2014). To find the initial permeability ellipsoid diameters, two institute permeability tests measuring two principal permeability values must be conducted; generally, one normal flow direction to the horizontal bedding plane and the other along with the bedding plane (assuming axisymmetry condition). However, due to axisymmetry, two major diameters of permeability ellipsoid are equal, so $B=C$. When measuring permeability on two perpendicular axes different from principal axes, knowing the two sets of direction cosines, the permeability ellipsoid can be built up. In this case, the geometry of the permeability ellipsoid is the same in both tests. However, different minor permeabilities provide the second relation between permeability ellipsoid parameters. The simultaneous solution of both equations presents the unknown parameters A, B, and C. Assuming the direction cosines of the advanced active planes in the first and second tests as and, respectively, A and B are calculated as follows:

$$\begin{cases} x_1^2 + y_1^2 + z_1^2 = K_v \\ x_1'^2 + y_1'^2 + z_1'^2 = K_h \end{cases} \quad (2)$$

$$\begin{cases} \frac{l^2 K_v}{B^2} + \frac{m^2 K_v}{B^2} + \frac{n^2 K_v}{A^2} = 1 \\ \frac{l'^2 K_h}{B^2} + \frac{m'^2 K_h}{B^2} + \frac{n'^2 K_h}{A^2} = 1 \end{cases} \quad (3)$$

where:

$$A = \frac{\sqrt{n'^2(l^2+m^2) - n^2(l'^2+m'^2)\cdot\sqrt{K_v K_h}}}{\sqrt{(l^2+m^2)K_v - (l'^2+m'^2)K_h}} \quad (4\text{-}1)$$

$$B = \frac{\sqrt{n'^2(l^2+m^2) - n^2(l'^2+m'^2)\cdot\sqrt{K_v K_h}}}{\sqrt{n^2 K_v - n'^2 K_h}} \quad (4\text{-}2)$$

Performing a plane strain case, the axe-symmetry condition is not available anymore. In preventing out-of-plane flow conductivity, the permeability ellipsoid is changed into an ellipse with no permeability to out-of-plane flow. In this case, the conservation of the minimum level of energy law forces the flow mechanism to occur in the plane. A two-dimensional flow is conducted, and the change in sliding orientation on an active plane, which is an active line, conducted from the first natural possible case, may make a necessity of being confined under constrained conditions. This may lead the crack widening/opening/sliding to face on local higher oriented permeability to change the flow regime.

To find out the values of internal permeability components of 13 planes oriented inside a certain permeability ellipsoid, first, the direction cosines of normal vectors as l'_i, m'_i, and n'_i are calculated as follows:

$$\beta_i = arctan\left|\frac{k_x}{k_y}\right| \quad (5\text{-}1)$$

$$\begin{Bmatrix} l'_i \\ m'_i \\ n'_i \end{Bmatrix} = \begin{bmatrix} \cos\beta_i & 0 & -\sin\beta_i \\ 0 & 1 & 0 \\ \sin\beta_i & 0 & \cos\beta_i \end{bmatrix} \begin{Bmatrix} l_i \\ m_i \\ n_i \end{Bmatrix} \quad (5\text{-}2)$$

The value of k_{ni} in direction l'_i, m'_i, and n'_i is obtained as follows:

$$k_{ni} = \frac{A.B}{\sqrt{(l_i'^2 + m_i'^2)A^2 + n_i'^2 B^2}} \quad (6)$$

The direction of calculated k_{xi}, k_{yi} on i^{th} plane is associated with a certain value of internal permeability k_{ni} in the permeability ellipsoid. This permeability can be obtained through the equation of intersected ellipse plane with permeability ellipsoid having the direction of k_{xi}, k_{yi} direction cosines. Simply, any change of k_{xi}, k_{yi} on planes, is faced on new permeability mechanism and ellipsoid. Therefore, the initial plane permeability matrix K_i^0 a 3 by 3 matrix composed of normal k_{ni} and k_{xi}, k_{yi} permeability components. The direction of calculated k_{xi}, k_{yi} on i^{th} plane is associated with a certain value of internal permeability k_{ni} in the permeability ellipsoid. This permeability can be obtained through the equation of intersected ellipse plane with permeability ellipsoid having the direction of k_{xi}, k_{yi} direction cosines. , any change of k_{xi}, k_{yi} on planes is faced on new permeability mechanism and ellipsoid. Therefore, the initial plane permeability matrix K_i^0 is a three-by-three matrix composed of normal k_{ni}, k_{xi}, *and* k_{yi} permeability components. Based on general mathematical matrix algebra, the initial permeability matrix of i^{th} plane can be calculated as follows:

$$K_i^{0G} = T_i^T K_i^0 T_i \quad (7)$$

K_i^{0G}, K_i^0, and T_i are the initial permeability matrix of i^{th} plane in the global coordinate, the initial permeability matrix of the same plane in the local coordinate, and *the* i^{th} plane transformation matrix, respectively.

6. Modeling Fracture/Crack Orientation

A multi-laminate-based model concept has been applied to analyze the influence of fracture–matrix interaction on the flow and transport processes on different scales. This implies that the single fracture and the adjacent matrix, the fracture orientation network, and the matrix in between are described rationally in space. The modeling setup includes several steps, which will be briefly outlined in the following. The first step in the multi-laminate modeling of fracture matrix–systems is the generation of a heterogeneous permeability field upon predefinition of sampling planes passing through a single point that the effects of any real fracture/crack with variable aperture can occur on these planes respectively. The corresponding opening/widening/sliding of all points through the porous medium simulates the generation of a fracture network (Peyman, F., & Sadrnejad, S. A. 2018 and Peyman, F. 2022 and Peyman, F., & Sadrnejad, S. A. 2017). The necessary geometry and material property database is gained from laboratory or field investigations and evaluated using not stochastic methods and geostatistical optimization tools but the real oriented values of each predefined sampling plane. Suppose the fracture density in the domain of interest is low. In that case, the initial values of different realizations of fracture networks with ellipsoidal properties are usually generated to fulfill the requirements of the ellipsoidal concept (Sadrnejad, S. A. 1992 and Sadrnejad, S. A., & PANDE, G. 1989).

The next step is the geometrical description of a plane fracture and its effects on permeability tensors with different impacts.

7. The Relation of On-Plane Permeability to Crack

Picandet et al. (2001) presented an empirical powered equation for permeability changes as follows:

$$K_i^D = K_i^0 . exp(\alpha D)^B \quad (8)$$

K_i^D and K_i^0 are damaged and initial permeability coefficients, respectively. α and B are two constants, and D is the damage function depending on crack geometry. The expansion of this equation leads to a plane permeability equation as follows:

$$K_i^D = K_i^0 . (1 + \alpha D)^B + \frac{(\alpha D)^{2B}}{2} + \frac{(\alpha D)^{3B}}{6} \quad (9)$$

According to Pijaudier-Cabot et al. (2009), the general permeability changes versus the strain ratio defining damage function for different types of concrete have been presented in Figure 5.

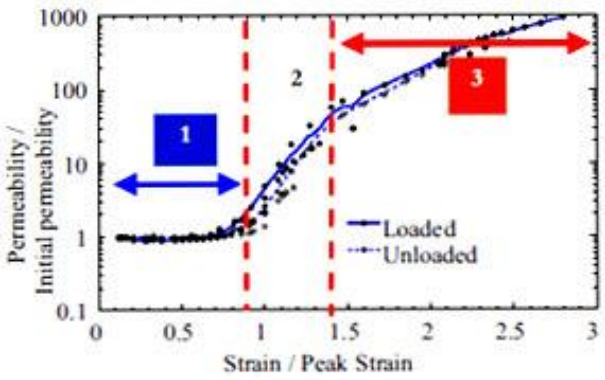

Fig, 5. Permeability changes vs. the strain ratio

A cracked sampling upon corresponding on-plane strain ratio as a damaged plane makes a local jumped value on the permeability ellipsoid of Gauss point to evaluate the crack effects of hydraulic conductivity. This local jump can be assumed to belong to a new higher level similar permeability ellipsoid with its diameters multiplied by $\sqrt{\varpi}$ that can be accounted as follows (Figure 6):

$$\begin{cases} \varpi = \dfrac{k_{ni(new)}}{k_{ni}} \\ k_{ni(new)} = \dfrac{\sqrt{\varpi}A.\sqrt{\varpi}B}{\sqrt{(l_i'^2 + m_i'^2)(\sqrt{\varpi}A)^2 + n_i'^2(\sqrt{\varpi}B)^2}} \end{cases} \quad (10)$$

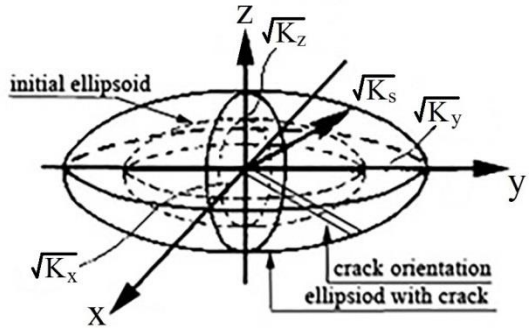

Fig,6. Initial, cracked affected ellipsoids

With this regard, calculating the i^{th} plane strain ratio, the damaged permeability matrix is provided, and the new permeability matrix of *the* i^{th} plane has been replaced to obtain the corresponding Gauss point permeability matrix in the FEM solution. The strain components and damage function for 13 planes can be computed using a multi-laminate damage model (Labibzadeh, M., Sadrnejad, S. A., 2006).

The governing equations for single-phase flow and transport in a saturated aquifer are the continuity equation combined with Darcy's law as follows:

$$S_0 \frac{\partial h}{\partial t} + div[(8\pi \sum_{i=1}^{n} w_i T_i^T K_i^D T_i)grad(h)] = q \quad (11)$$

Therefore, the advection-dispersion transport–equation employed is as follows:

$$\frac{\partial c}{\partial t} + div(cv) - div[(8\pi \sum_{i=1}^{n} w_i T_i^T K_i^D T_i)grad\, c)] = r \quad (12)$$

where S_0 represents the specific storage coefficient, h the piezometric head, t the time, K_i^D the hydraulic conductivity tensor for i^{th} plane, c the solute concentration, v the seepage velocity, q flow flux, r externally applied source and sink terms, T_i is transformation matrix for i^{th} plane and n is number of sampling planes. The permeability matrix K_i^D for i^{th} plane is a 3×3 matrix in Cartesian coordinate of i^{th} plane, including the effects of strain tensor variations of corresponding plane. The transformation matrix is defined for three perpendicular planes at global Cartesian coordinate of each Gauss points; therefore, T_i for each set of three planes corresponding to i^{th} plane is as follows:

Where S_0 represents the specific storage coefficient, h the piezometric head, t the time, K_i^D the hydraulic conductivity tensor for i^{th} plane, c the solute concentration, v the seepage velocity, q flow flux, r externally applied source and sink terms, Ti is transformation matrix for i^{th} plane and n is number of sampling planes. The permeability matrix K_i^D for the i^{th} plane is a 3×3 matrix in the Cartesian coordinate of the i^{th} plane, including the effects of strain tensor variations of the corresponding plane. The transformation matrix is defined for three perpendicular planes at the global Cartesian coordinate of each Gauss point; therefore, Ti for each set of three planes corresponding to the i^{th} plane is as follows:

$$[T_i] = \begin{bmatrix} L_{x_i'x} & L_{x_i'y} & L_{x_i'z} \\ L_{y_i'x} & L_{y_i'y} & L_{y_i'z} \\ L_{z_i'x} & L_{z_i'y} & L_{z_i'z} \end{bmatrix} \cdot \begin{bmatrix} l_i & 0 & 0 & m_i & 0 & n_i & 0 & 0 & 0 \\ 0 & m_i & 0 & 0 & l_i & 0 & 0 & n_i & 0 \\ 0 & 0 & n_i & 0 & 0 & 0 & l_i & 0 & m_i \end{bmatrix} \quad (13)$$

Based on the description of local axes and the relations for transforming stress tensor to a sampling plane, it is enough to multiply the transformation matrix by a rotation matrix to be presented in i^{th} plane local axis. Therefore, L is the rotation matrix, and x'_i, y'_i, and z'_i are the local axes of i^{th} plane as follows:

$$T_i = \begin{bmatrix} L_{x_i'x} & L_{x_i'y} & L_{x_i'z} \\ L_{y_i'x} & L_{y_i'y} & L_{y_i'z} \\ L_{z_i'x} & L_{z_i'y} & L_{z_i'z} \end{bmatrix} \cdot \begin{bmatrix} l_i & 0 & 0 \\ 0 & m_i & 0 \\ 0 & 0 & n_i \end{bmatrix} \quad (14)$$

Summing up the permeability matrices tensors of all sampling planes, a numerical integration rule and corresponding transformed weighted matrix of all planes must be employed as follows:

$$K_{Gauss}^D = 8\pi \sum_{i=1}^{n} w_i T_i^T K_i^D T_i \quad (15)$$

8. Cracks in Sefid-Rood Buttressed Dam by Earthquake

This dam's height is 106 m. with 417 m. of crest length. It was built between 1956 and 1963 in Gilan state, north of Iran. Due to earthquake magnitude 7.3, Richter 1990 rib base no.18 of this dam cracked, and some seepage started, as shown in Figure 7, which was later amended by resin injection. This rib base was modeled through a developed computer program, and the internal damages and permeability changes were predicted, as well as pore water pressure, and compared with what was observed after damage by the earthquake.

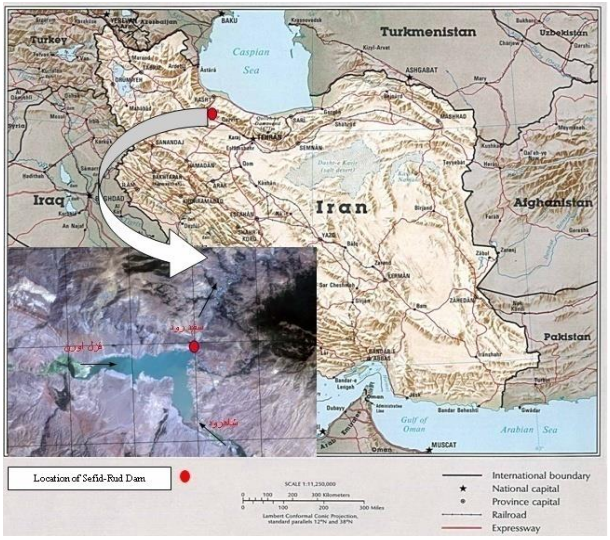

(a)

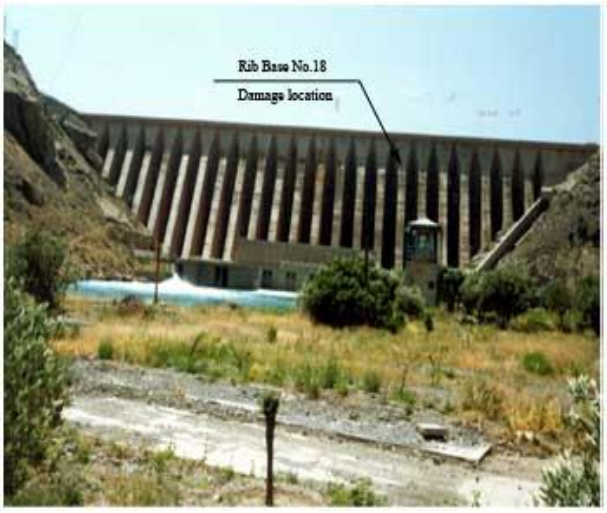

(b)

Fig.7. a) Location of Sefid-Rood dam in Iran b) Sefid-Rood dam downstream view

Figure 8 presents Rudbar's (1990) earthquake acceleration three components. Figures 9 and 10 show the dam plan and rib number 18 details.

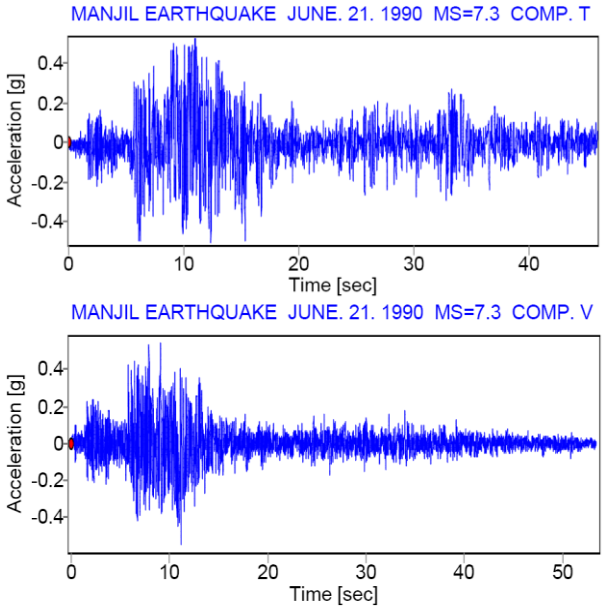

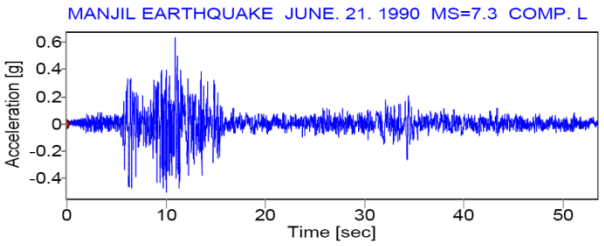

Fig.8. Normalized earthquake components

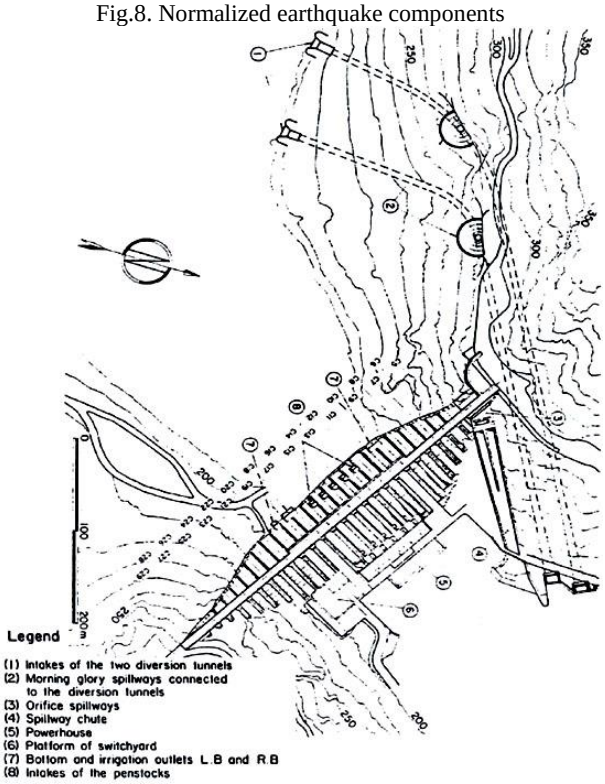

Fig.9. Sefid-Rood dam plan and its location

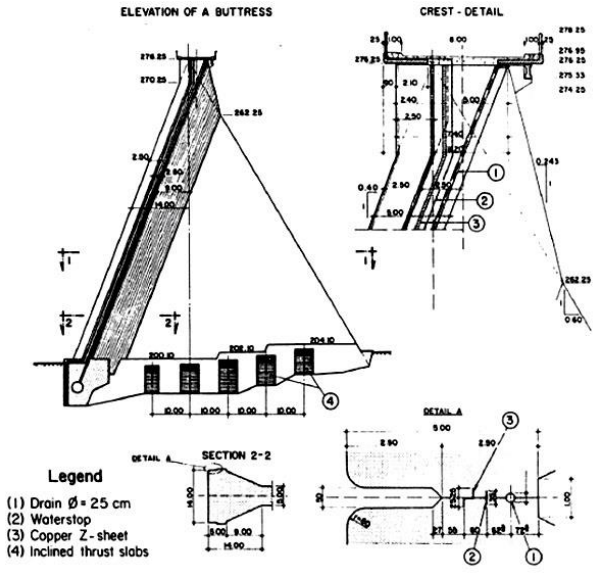

Fig.10. Rib No.18 details in Sefid-Rood dam

The downstream crack view due to the earthquake is shown in Figure 11. The crack location and components are shown in Figure 12. The mechanical properties of concrete are shown in Table 2. Figure 13 shows tensile strength and compares compressive test results of concrete.

Fig.11. Downstream cracks view of rib number 18

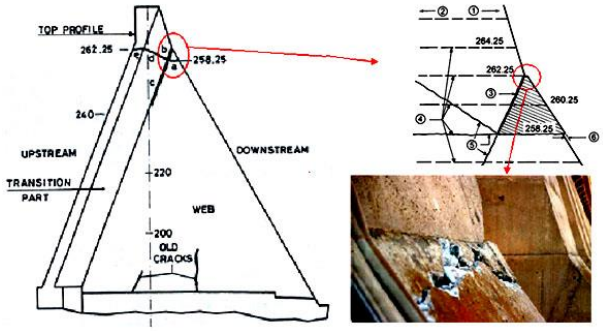

Fig.12. Cracks details

Table 2 Concrete properties

Dynamic Young Modulus $E_d(MPa)$	Elastic Young Modulus $E(MPa)$	Poisson' ratio ν	Mass per unit volume $\rho(kg/m^3)$	Compressive strength $f'_c(MPa)$
29000	20000	0.17	2250	16.9

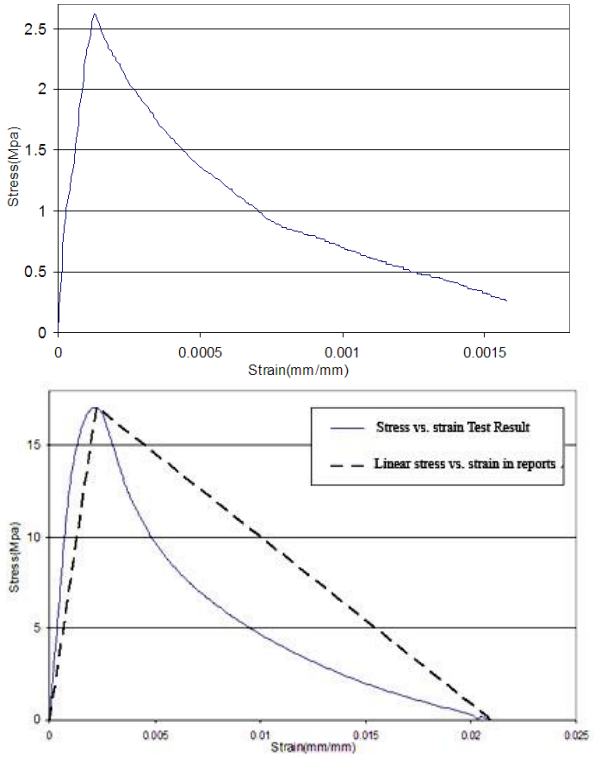

Fig.13. Tensile and compressive test results on concrete

The FE-mapped mesh of rib number 18, including the first cracked locations, is shown in Figure 14. The first failed plane number 8 at node 85, as combined stress and normal strain time histories are presented in Figures 15 and 16. Plane no. 8 of node 85 normal stress vs. strain, its time history, its stress path, and the orientation of this failed plane are presented in Figures 17 and 18.

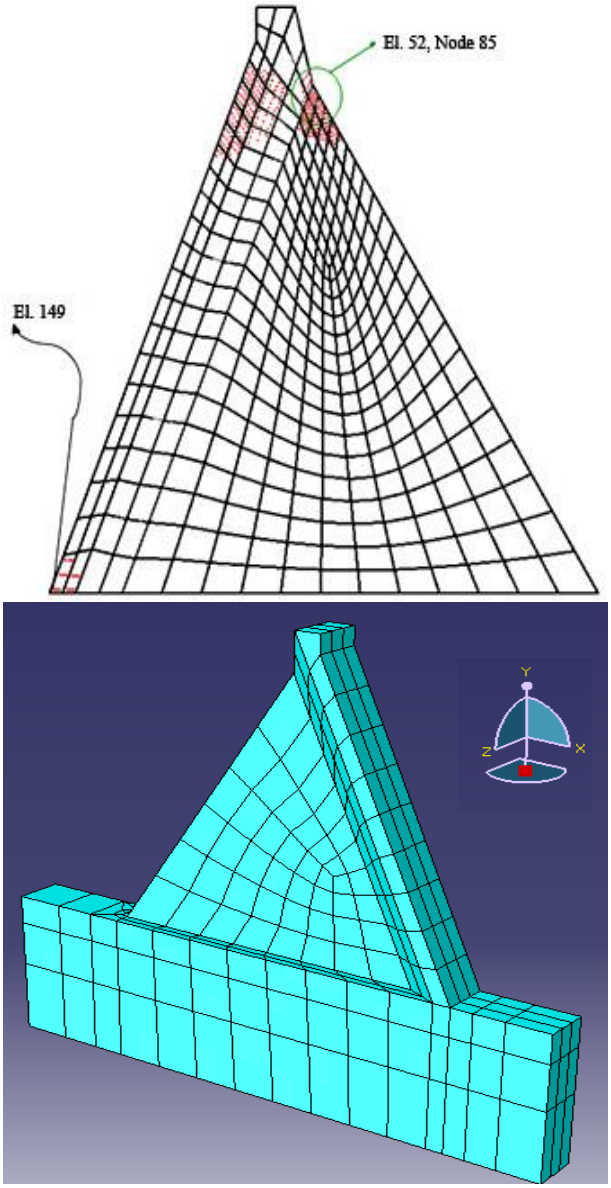

Fig.14. Maped elements and damaged locations

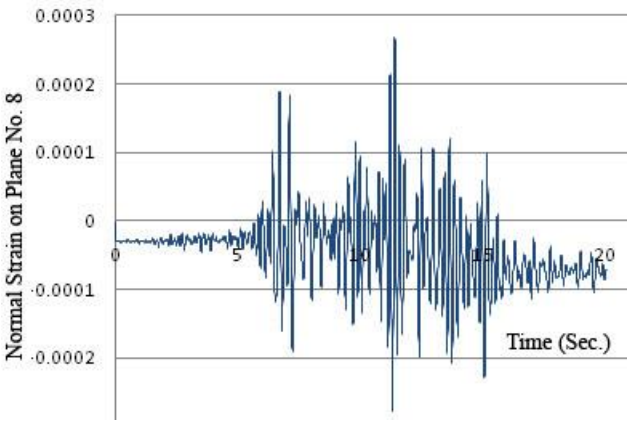

Fig.15. Predicted combined stress variation at Node 85, Plate No. 8 (The first failed plane)

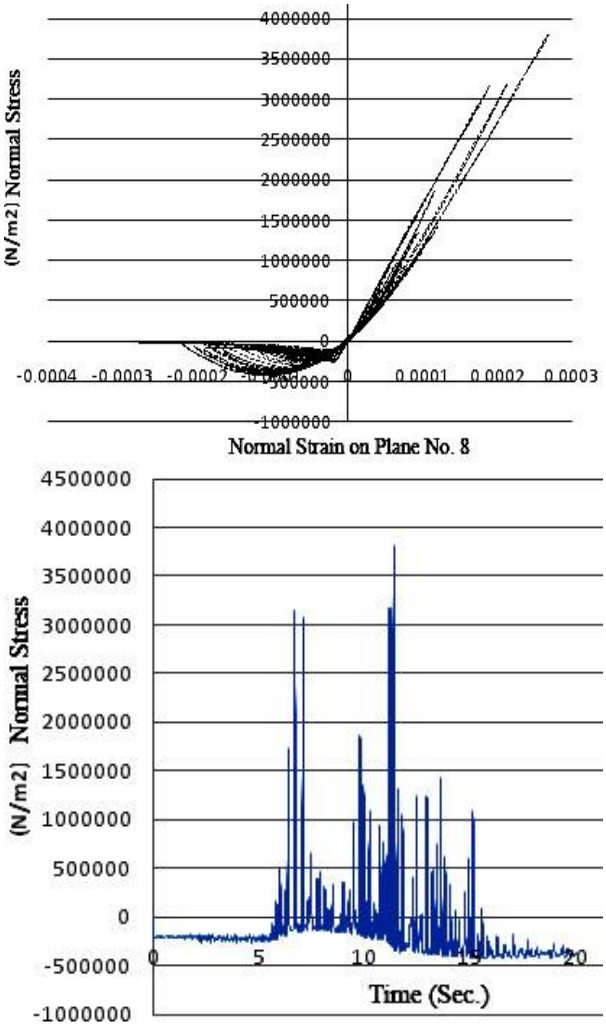

Fig.17. Normal stress vs. strain and time history of Normal stress on plane no. 8 of Node 85

Figure 19 shows pore water pressure contours and the comparison of measured hydrostatic p.w.p. at the piezometer locations after 4 seconds since the start of the earthquake with model results. The pore water pressure contours at the end of an earthquake are predicted in Figure 20. To show the capability of the proposed model, the two measured pore water pressure histories at piezometer no. 139 and 435 during earthquakes are compared with model results in Figure 21. This comparison reveals that the proposed model can predict such dynamic results during and after the earthquake.

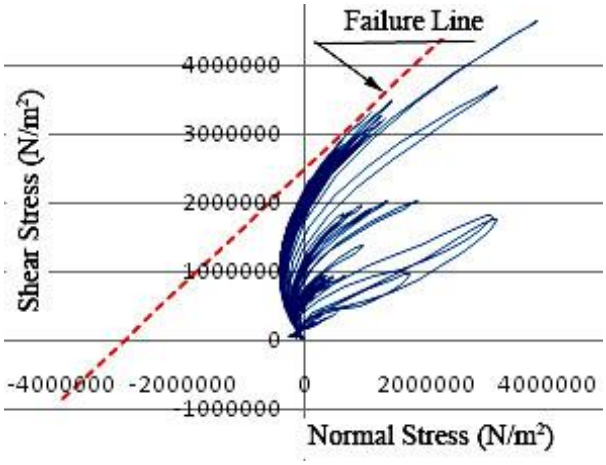

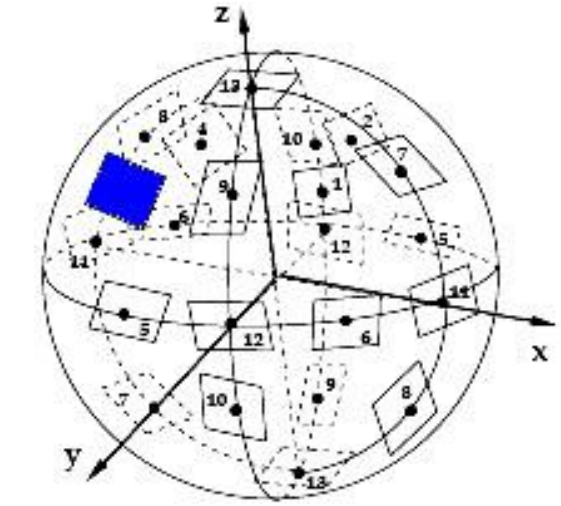

Fig.18. Stress path on plane no. 8 and its direction on the sphere

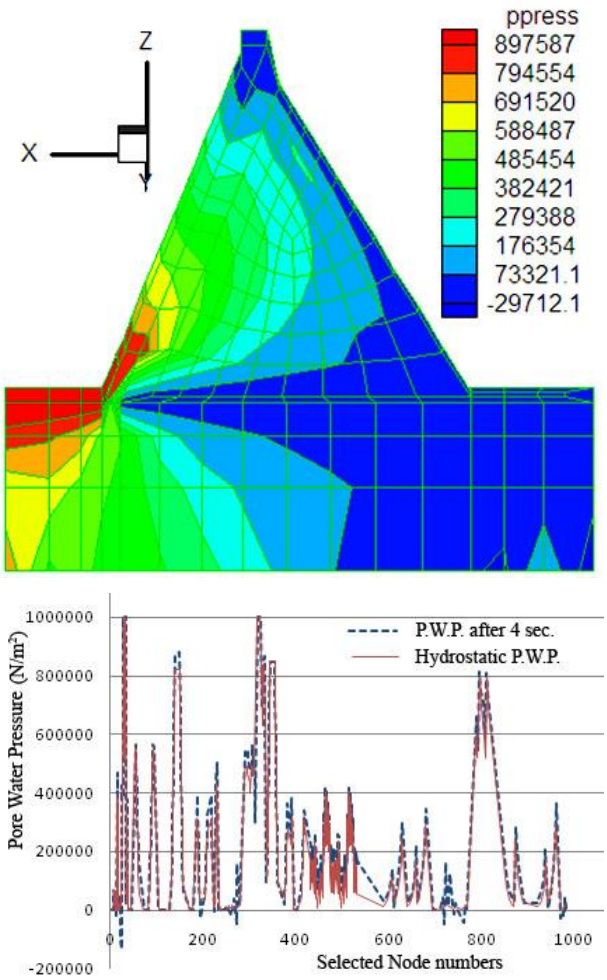

Fig.19. Pore water pressure contours and hydrostatic–developed p.w.p. after 4 seconds

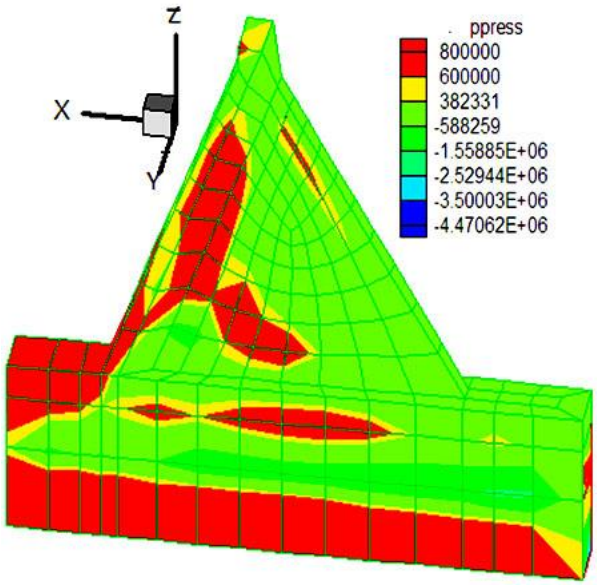

Fig.20. Final Pore water pressure contours through the dam body

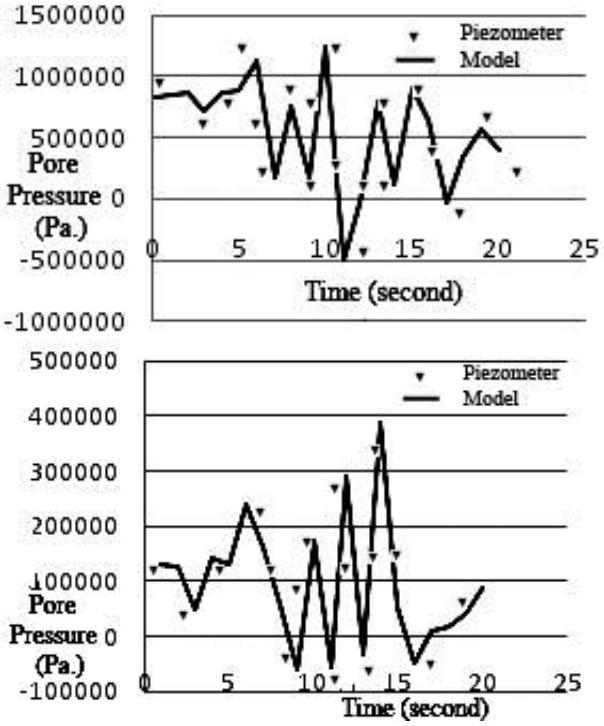

Fig.21. Pore water pressure at piezometer No. 139 and 435 during an earthquake

9. Conclusions

A damage permeability tensor of multi-laminate model concept containing crack effect and fracture generation upon multi-laminate frame word and numerical integration techniques has been developed and employed to examine the influence of fracture–matrix–interaction on flow and transport processes and the corresponding effective parameters in fractured systems concerning different scales. The results of the fractured concrete dam presented in this research have shown that, depending on the mechanical properties, the presence of a fractured matrix in a fractured system leads to a considerable conductivity matrix change affecting pore water pressure and the flow and transport conditions through a cracked concrete medium. A simple multi-laminate technique has been employed to evaluate crack opening displacement. This led to the minimum energy level failure mechanism analyses and permeability tensor change based on the orientation damage model. Suppose the on-plane strain distributions are close as the regularized effective strain derived from a nonlocal (integral or gradient) model and the regularized effective strain derived from a strong discontinuity. In that case, the permeability variation controlled by cracks has reached a distribution close to that of real crack effects. The corresponding distribution of the continuous nature of flow is expected to be close to that resulting from a predicted discontinuity (crack) in a regularized, nonlocal analysis.

An alternative averaging technique – the same as the integral model – has been devised to compare effective strain distributions leading to permeability tensor changes. The quality of the crack opening estimate depends on the weight function that enters the nonlocal expression, affecting flow transfer through cracked porous media. The flow gradient approach is equivalent to a nonlocal average with a sharper distribution, lending less weight to neighboring points than the non-uniform Gaussian distribution in the classical integral approach. Consequently, the gradient approach provides better limit values of the quality for a formed crack than with the integral model.

References

[1] Choinska, M., Khelidj, A., Chatzigeorgiou, G., & Pijaudier-Cabot, G. (2007). Effects and interactions of temperature and stress-level related damage on permeability of concrete. *Cement and Concrete Research*, *37*(1), 79-88.

[2] Comi, C., Mariani, S., & Perego, U. (2007). An extended FE strategy for transition from continuum damage to mode I cohesive crack propagation. *International Journal for Numerical and Analytical Methods in Geomechanics*, *31*(2), 213-238.

[3] Dagan, G. (2012). *Flow and transport in porous formations*. Springer Science & Business Media.

[4] Hearn, N. (1999). Effect of shrinkage and load-induced cracking on water permeability of concrete. *Materials Journal*, *96*(2), 234-241.

[5] Hearn, N., & Lok, G. (1998). Measurement of permeability under uniaxial compression: a test method. *Materials Journal*, *95*(6), 691-694.

[6] Hillerborg, A., Modéer, M., & Petersson, P. E. (1976). Analysis of crack formation and crack growth in concrete by means of fracture mechanics and finite elements. *Cement and concrete research*, *6*(6), 773-781.

[7] Labibzadeh, M., & Sadrnejad, S. A. (2006). Mesoscopic damage based model for plane concrete under static and dynamic loadings. *American Journal of Applied Sciences*, *3*(9), 2011-2019.

[8] Larsson, R., Steinmann, P., & Runesson, K. (1999). Finite element embedded localization band for finite strain plasticity based on a regularized strong discontinuity. *Mechanics of Cohesive-frictional Materials: An International Journal on Experiments, Modelling and Computation of Materials and Structures*, *4*(2), 171-194.

[9] Long, J. C. (1983). *Investigation of equivalent porous medium permeability in networks of discontinuous fractures*. University of California, Berkeley.
[10] Oliver, J., Huespe, A. E., Pulido, M. D. G., & Chaves, E. (2002). From continuum mechanics to fracture mechanics: the strong discontinuity approach. *Engineering fracture mechanics*, *69*(2), 113-136.
[11] Peerlings, R. H., de Borst, R., Brekelmans, W. M., & de Vree, J. (1996). Gradient enhanced damage for quasi-brittle materials. *International Journal for numerical methods in engineering*, *39*(19), 3391-3403.
[12] Peerlings, R. H., Geers, M. G., de Borst, R., & Brekelmans, W. (2001). A critical comparison of nonlocal and gradient-enhanced softening continua. *International Journal of solids and Structures*, *38*(44-45), 7723-7746.
[13] Peyman, F. (2022). Investigation of Failure Mechanism in Earth Dam upon Triggered Liquefaction. *Analytical and Numerical Methods in Mechanical Design*, *1*(2), 39-57.
[14] Peyman, F. (2022). Investigation of The Mechanism of Change of Concrete Modulus Matrix in Monotonic Loading and its Numerical Analysis. *Analytical and Numerical Methods in Mechanical Design*, *1*(1), 73-89.
[15] Peyman, F. (2022). Numerical analysis of the behavior of undrained sands in monotonic loading based on standardization of experimental results. *Asas Journal*, *24*(67).
[16] Peyman, F., & Sadrnejad, S. A. (2017). Liquefied Residual Strength of Undrained Sand upon A Parametric Approach to Hypo-elastic Model. *Numerical Methods in Civil Engineering*, *2*(1), 49-60.
[17] Peyman, F., & Sadrnejad, S. A. (2018). Analysis of concrete crack growth based on micro-plane model. *Structural Concrete*, *19*(3), 930-945.
[18] Picandet, V., Khelidj, A., & Bastian, G. (2001). Effect of axial compressive damage on gas permeability of ordinary and high-performance concrete. *Cement and concrete research*, *31*(11), 1525-1532.
[19] Pijaudier-Cabot, G. and Bazant, Z. (1987), "Nonlocal damage theory", J. of Eng. Mech., 113, 1512-1533.
[20] Pijaudier-Cabot, G., & Jason, L. (2002). Continuum damage modelling and some computational issues. *Revue française de genie civil*, *6*(6), 991-1017.
[21] Pijaudier-Cabot, G., Dufour, F., & Choinska, M. (2009). Permeability due to the increase of damage in concrete: From diffuse to localized damage distributions. *Journal of engineering mechanics*, *135*(9), 1022-1028.
[22] Sadrnejad, S. A. (1992). Multilaminate elastoplastic model for granular media. *International Journal of Engineering*, *5*(1), 11-24.
[23] Sadrnejad, S. A. (1992, June). Induced anisotropy prediction through plasticity. In *Proceeding of international conference on engineering applications of mechanics* (pp. 598-605).
[24] Sadrnejad, S. A. (2014). A constitutive model for shape memory alloys, visualizing internal deformability mechanism. In *Construction Materials and Structures* (pp. 1223-1232). IOS Press.
[25] Sadrnejad, S. A., & Labibzadeh, M. (2006). Dynamic solution code for structural analysis upon joint element. *J. Comput. Sci*, *2*, 401-409.
[26] Sadrnejad, S. A., & PANDE, G. (1989). A MULTILAMINATE MODEL FOR SANDS. NUMERICAL MODELS IN GEOMECHANICS. NUMOG III. PROCEEDINGS OF THE 3RD INTERNATIONAL SYMPOSIUM HELD AT NIAGARA FALLS, CANADA, 8-11 MAY 1989. *Publication of: Elsevier Applied Science Publishers Limited*.
[27] Simo, J. C., Oliver, J. A. V. I. E. R., & Armero, F. (1993). An analysis of strong discontinuities induced by strain-softening in rate-independent inelastic solids. *Computational mechanics*, *12*(5), 277-296.
[28] Simone, A., Wells, G. N., & Sluys, L. J. (2003). From continuous to discontinuous failure in a gradient-enhanced continuum damage model. *Computer Methods in Applied Mechanics and Engineering*, *192*(41-42), 4581-4607.
[29] Sugiyama, T., Bremner, T. W., & Holm, T. A. (1996). Effect of stress on gas permeability in concrete. *Materials Journal*, *93*(5), 443-450.
[30] Wollrath, J. (1990). *Ein Strömungs-und Transportmodell für klüftiges Gestein und Untersuchungen zu homogenen Ersatzsystemen* (Doctoral dissertation, Inst. für Strömungsmechanik und Elektron. Rechnen im Bauwesen).